Journal of Power Sources 370 (2017) 27–35

Contents lists available at ScienceDirect

Journal of Power Sources

journal homepage: www.elsevier.com/locate/jpowsour

Determination of the core temperature of a Li-ion cell during thermal runaway

M. Parhizi, M.B. Ahmed, A. Jain*

Mechanical and Aerospace Engineering Department, University of Texas at Arlington, Arlington, TX, USA

HIGHLIGHTS

- Develops a method to determine core temperature of Li-ion cell in thermal runaway.
- Predictions from method validated through experiments in a broad parameter space.
- Core temperature found to exceed surface temperature by 100s of degrees Celsius.
- Results help determine the thermal state of a cell during thermal runaway.
- Results may help understand and develop strategies to mitigate thermal runaway.

ARTICLE INFO

Article history:
Received 5 July 2017
Received in revised form
27 September 2017
Accepted 30 September 2017

Keywords:
Lithium ion battery
Safety
Thermal runaway
Core temperature
Thermal modeling

ABSTRACT

Safety and performance of Li-ion cells is severely affected by thermal runaway where exothermic processes within the cell cause uncontrolled temperature rise, eventually leading to catastrophic failure. Most past experimental papers on thermal runaway only report surface temperature measurement, while the core temperature of the cell remains largely unknown. This paper presents an experimentally validated method based on thermal conduction analysis to determine the core temperature of a Li-ion cell during thermal runaway using surface temperature and chemical kinetics data. Experiments conducted on a thermal test cell show that core temperature computed using this method is in good agreement with independent thermocouple-based measurements in a wide range of experimental conditions. The validated method is used to predict core temperature as a function of time for several previously reported thermal runaway tests. In each case, the predicted peak core temperature is found to be several hundreds of degrees Celsius higher than the measured surface temperature. This shows that surface temperature alone is not sufficient for thermally characterizing the cell during thermal runaway. Besides providing key insights into the fundamental nature of thermal runaway, the ability to determine the core temperature shown here may lead to practical tools for characterizing and mitigating thermal runaway.

1. Introduction

Li-ion cells offer an excellent mechanism for electrochemical energy storage and conversion, with superior energy storage and power density compared to predecessor technologies [1–4]. However, the performance of Li-ion cells is known to be highly sensitive to temperature [5,6], and even modest rise in operating temperature results in severe safety and reliability concerns. Fundamentally, high temperature triggers multiple exothermic reactions and processes inside a Li-ion cell, such as degradation of separator, reaction between the anode active material and electrolyte, reaction between the positive active material and electrolyte and finally electrolyte decomposition [7–10]. As the cell temperature rises due to such processes, the rates of heat generation increase even more [11]. In addition, newer, more exothermic reactions are also triggered. This chain mechanism continues until the heat generation rate becomes unsustainably large, thereby pushing the cell into a catastrophic thermal runaway situation. Thermal runaway is a significant technological challenge that has been investigated in a large body of experimental and theoretical research [7,8,10–16].

A number of experimental techniques have been used for

* Corresponding author. 500 W First St, Rm 211, Arlington, TX 76019, USA.
E-mail address: jaina@uta.edu (A. Jain).

https://doi.org/10.1016/j.jpowsour.2017.09.086
0378-7753/

investigating the nature of thermal runaway in Li-ion cells [8,10,15]. Reactions and processes leading to thermal runaway are usually modeled based on Arrhenius kinetics. Reaction rate parameters for these processes have been experimentally determined [8,17]. Heat generation rates have been measured in both nominal and runaway conditions using both calorimetric and non-calorimetric techniques [12,18,19]. At the cell level, thermal runaway has been induced through a variety of mechanisms including nail penetration, internal short circuit, high temperature oven tests, etc. [5,6,10,13,20]. In each case, the surface temperature of the cell has been measured and used as a metric to represent the thermal health of the cell. Surface temperature measurement has been carried out through both contact and non-contact techniques such as thermocouples and infrared thermography respectively [10,13,21–24]. Threshold values for the surface temperature for inducing a thermal runaway have been determined experimentally [10,12,13]. The fundamental processes that contribute towards thermal runaway, including temperature-dependent heat generation, thermal conduction and convection have been combined into a single non-dimensional number [11]. A threshold value for this number has been shown to exist, above which thermal runaway is imminent.

The risk of thermal runaway is usually managed by battery management approaches such as load reduction on the cell when its temperature exceeds a certain threshold. While this approach may keep the cell safe, it usually comes at the cost of performance. The effectiveness of this significant trade-off between safety and performance depends critically on accurate measurement of the cell temperature, which is a key indicator of the thermal health of the cell and a predictor of the onset of thermal runaway. Surface temperature measurement, while providing some indication of the thermal state of the cell, is not completely representative, since the internal temperature at the core of the cell may be much higher due to internal heat generation [18] and poor thermal conductivity [25] of the cell. The higher, internal temperature may drive thermal runaway even when the surface temperature is much lower. Information about the core temperature is therefore critical for fully understanding and alleviating thermal runaway. Any technique to manage thermal runaway based on surface temperature alone is likely to be in significant error, as the core temperature – and not the surface temperature – is an appropriate indicator of the thermal state of the cell.

Most past papers have only measured cell temperature on the outer surface [10,12,13] and not the core temperature, possibly due to the several challenges associated with core temperature measurement, such as the hermetically sealed nature of the cell and lack of physical access to the core. A limited number of techniques that have been evaluated for measuring the internal temperature of the cell include fiber Bragg gratings [26], temperature measurement through electrochemical parameter measurement [27] and even micro-thermocouples [28,29]. Limited work exists on internal temperature measurement using embedded thermocouples during short circuit and overcharge conditions [29], wherein a significant temperature difference between internal temperature and external surface temperature was reported. This work reported internal temperature of up to 195 °C for $LiCoO_2$ cells in mild abuse conditions [29], although temperature during a thermal runaway event that causes fire and explosion is expected to be much higher. Several of these techniques require physical insertion of a sensor into the cell, which often leads to cell failure and is unlikely to work well for widespread implementation. Others, such as electrochemistry based temperature measurement only provide an average temperature of the cell, and not the peak temperature. In the recent past, a method for predicting the internal temperature of a cylindrical Li-ion cell based on measurement of the surface temperature has been developed [21,22]. This method requires information about the heat generation rate and thermophysical properties of the cell, and has been experimentally demonstrated for nominal, non-runaway operating conditions. Given the technological importance of predicting, managing and preventing thermal runaway, it is of much interest to extend such methods for measurement of the internal temperature of the cell during extreme conditions encountered in thermal runaway. Any such effort will help understand the thermal state inside the cell during thermal runaway and will positively impact the fundamental understanding and practical management of thermal runaway in Li-ion cells.

This paper presents an experimentally validated method for determining the core temperature of a cylindrical Li-ion during thermal runaway. This technique is based on measured surface temperature data as a function of time and chemical reaction kinetics during thermal runaway. These data are used in an analytical heat transfer model to determine the core temperature as a function of time. The core temperature determined in this manner is found to be in good agreement with experimental measurements on a thermal test cell undergoing a thermal process that mimics thermal runaway in real cells. The technique is used to determine the core temperature as a function of time for a number of surface temperature measurements reported in past papers. In each case, it is found that the peak core temperature is several hundred degrees Celsius higher than the surface temperature. This provides a critical, previously unavailable insight into the thermal state inside the cell, which is not possible through surface temperature measurement alone. The capability for determining the core temperature of the cell during thermal runaway, enabled by this work, may contribute towards an improved fundamental understanding of thermal runaway, as well as practical techniques for improved safety of Li-ion cells through effective management of thermal runaway risks.

2. Mathematical modeling

Fig. 1(a) shows a schematic of the geometry considered here, comprising a cylindrical Li-ion cell of radius R. Radial thermal conductivity and diffusivity of the cell are assumed to be k_r and α respectively. Internal heat generation within the cell, $Q(T)$, which occurs due to various electrochemical processes, is a function of temperature. Surface temperature at the outer surface, $r=R$, is assumed to be known from experimental measurements, as reported in several past papers [10,12,13]. The interest here is to develop a model to predict the evolution of the core temperature based on the measured surface temperature and the internal heat generation. In the cylindrical coordinate system used here, it is possible to derive a governing partial differential equation for the temperature rise $T(r,t)$ by considering energy conservation of an infinitesimally small element [30,31]. By accounting for thermal conduction into and out of this element, as well as internal heat generation and energy storage, the energy equation, used commonly for heat transfer analysis, can be found to be

$$\left(\frac{\partial^2 T}{\partial r^2}+\frac{1}{r}\frac{\partial T}{\partial r}\right)+\frac{Q(T)}{k_r}=\frac{1}{\alpha}\frac{\partial T}{\partial t} \tag{1}$$

Boundary conditions associated with equation (1) are

$$\frac{\partial T}{\partial r}=0 \quad \text{at } r=0 \tag{2}$$

and

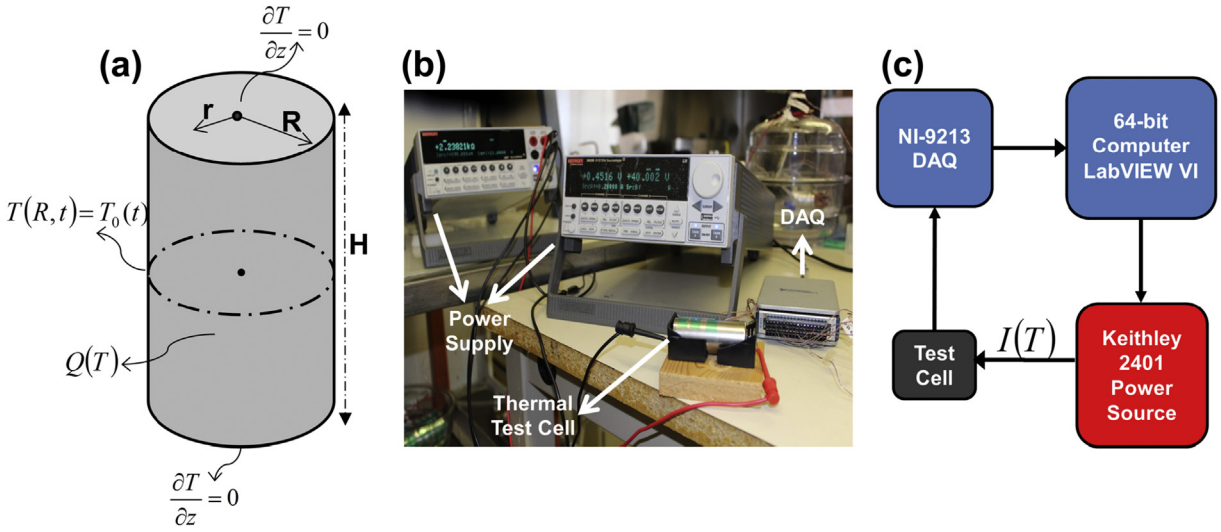

Fig. 1. (a) Schematic of the problem, (b) Picture, and (c) Schematic of the experimental setup.

$$T = T_0(t) \quad \text{at } r = R \tag{3}$$

Temperature rise at $t = 0$ is assumed to be zero. Temperature-dependent heat generation in equation (1) and time-dependent surface temperature in equation (3) are the two non-homogeneities in this problem. In order to derive a solution, the problem is first divided into two sub-problems, $T_1(r,t)$ and $T_2(r,t)$ that account for each non-homogeneity separately. $T_1(r,t)$ represents the temperature rise due to internal heat generation alone, and $T_2(r,t)$ represents the temperature rise due to time-dependent surface temperature alone.

The solution for $T_1(r,t)$ depends on the nature of internal heat generation $Q(T)$. Heat generation during thermal runaway is usually modeled as an Arrhenius function

$$Q = Q_o \exp\left(\frac{-E_a}{R_u T}\right) \tag{4}$$

Where Q_0 is the pre-exponential constant, E_a is the activation energy and R_u is the universal gas constant.

Due to the exponential nature of temperature dependence of Q, the governing energy equation for $T_1(r,t)$ is highly nonlinear, and consequently very difficult to solve. Linearization through time-stepping is carried out in order to solve for $T_1(r,t)$. The time duration of interest is divided into a number of smaller time intervals, for which $T_1(r,t)$ is computed in a sequential fashion. Each time interval is chosen to be small enough, such that the change in heat generation due to increased temperature during the interval is reasonably small. This allows the $Q(T)$ term to be considered to be constant during each time interval. Based on linearization of the problem in this fashion, the temperature distribution $T_1(r,t)$ during each time interval can be computed using the method of separation of variables techniques. The solution for $T_1(r,t)$ is found to be

$$T_1(r,t) = s(r) + w(r,t) \tag{5}$$

Where

$$s(r) = \frac{Q_{gen}}{4k}\left(R^2 - r^2\right) \tag{6}$$

and

$$w(r,t) = \sum_{n=1}^{\infty} A_n J_0(\lambda_n r)\exp\left(-\alpha\lambda_n^2 t\right) \tag{7}$$

where A_n is given by

$$A_n = \frac{\int_0^R r(T_{initial}(r) - s(r))J_0(\lambda_n r)dr}{\int_0^R rJ_0(\lambda_n r)^2 dr} \tag{8}$$

where the eigenvalues λ_n are given by the roots of J_0, the Bessel function of the first kind and of order zero.

Note that Q_{gen} is the heat generation rate during the specific time interval, and $T_{initial}(r)$ is the temperature distribution in the cell at the start of the time interval, which must be determined by computing the temperature distribution during the immediately preceding time interval. Equations (5) through (8) provide an approach for handling the non-linearity in the equations for $T_1(r,t)$ and computing the temperature distribution in a recursive fashion.

This linearization approach introduces approximations in the temperature distribution because it assumes the heat generation rate to be uniform throughout the cell. Further, because the temperature distribution in the cell may be non-uniform due to the low thermal conductivity of the cell [25], it is important to determine the temperature at which to compute the heat generation rate for each time interval. These limitations of the linearization approach can be minimized by choosing the time intervals to be sufficiently short.

Deriving an expression for $T_2(r,t)$ is relatively simpler, and is similar to a procedure outlined in a recent paper [21]. Using the method of undetermined parameters, $T_2(r,t)$ is found to be

$$T_2(r,t) = \sum_{n=1}^{\infty} B_n(t)J_0(\lambda_n r) \tag{9}$$

where $B_n(t)$ is given by

$$B_n(t) = \frac{\alpha\lambda_n R J_1(\lambda_n R)}{N_{r,n}} \int_0^t T_0(\tau)\exp\left[-\alpha\lambda_n^2(t-\tau)d\tau\right] \quad (10)$$

and the radial norm $N_{r,n}$ is

$$N_{r,n} = \frac{R^2 J_1(\lambda_n R)^2}{2} \quad (11)$$

Equations (9) through (11) show that $T_2(r,t)$ can be determined by appropriately integrating the measured surface temperature $T_0(t)$.

Finally, by combining $T_1(r,t)$ and $T_2(r,t)$, the core temperature of the cell $T_{core}(t)$ can be computed as follows

$$T_{core}(t) = T_1(0,t) + T_2(0,t) \quad (12)$$

Note that determining the core temperature of the cell during thermal runaway using the method outlined above requires information about the temperature-dependent heat generation rates during runaway, as well as thermal properties of the cell. These parameters are generally available in several past papers. Heat generation rates are usually modeled using the Arrhenius equation and the various associated Arrhenius parameters have been determined and reported in past papers [7,8,10]. On the other hand, thermal properties of a Li-ion cell, including thermal conductivity and specific heat have also been measured [18] as well as estimated from theoretical models [19].

3. Experiments

3.1. Thermal test cell

Experiments are carried out to validate the analytical model for determining the core temperature of a cell as presented in section 2. Note that imposing and measuring a precise, well-controlled temperature-dependent heat generation rate in a Li-ion cell is not straight forward. Further, there is a lack of experimental methods to directly measure the core temperature, in part due to its hermetically sealed nature. As a result, these experiments are carried out on a thermal test cell that is carefully designed and fabricated in order to closely match the geometry and thermal transport properties of a 26650 Li-ion cell. Fabrication and measurements on such thermal test cells have been described in recent papers [11,21,22]. In short, the thermal test cell comprises a rolled, thin resistive 304 stainless steel foil placed inside a 26650 cell casing. Thermocouples are placed at different radii, including at the core and surface of the roll for temperature measurement. Heat is generated inside the cell by passing electrical current through the resistive metal foil. Temperature-dependence of heat generation rate is implemented by monitoring the cell temperature through embedded thermocouples and changing the heating current in order to implement any desired $Q(T)$ expression, as shown schematically in Fig. 1(c).

3.2. Experimental setup

Fig. 1(b) shows a picture of the experimental setup, comprising the thermal test cell, T-type thermocouples, a NI-9213 data acquisition system (DAQ), Keithley 2401 power sources and LabView software running on a 64-bit computer. Fig. 1(c) shows a schematic of the flow of information during the experiment.

Core temperature of the thermal test cell is measured at 1 s intervals by LabVIEW software through the NI-9213 DAQ. The heat generation rate to be imposed in the cell is determined using the measured temperature and the desired temperature dependence, $Q(T)$. The amount of current needed for the heat generation rate is determined based on the electrical resistance of the metal foil and supplied to the thermal test cell by the Keithley 2401 power sources. Surface temperature of the thermal test cell is measured every 1 s. Experiments are repeated by changing the $Q(T)$ expression implemented in the heat generation feedback loop for multiple values of Q_0 and E_a. In each case, measured core temperature is compared against predictions from the analytical model from Section 2.

In addition to experiments described above, analysis of experimental data on 18650 cells reported in three past papers [10,12,13] is also carried out. Section 4 shows that specific heat of the 18650 cell is a critical parameter in these computations. As a result, experiments are carried out to independently measure the specific heat of an 18650 Li-ion cell.

To do so, a completely discharged 18650 Li-ion cell is heated up to 45 °C inside a BOEKEL incubator. Surface temperature of the cell is measured using Omega T-type thermocouples connected to a NI-9213 data acquisition system and controlled by LabView software. Once the cell reaches a steady temperature, it is placed inside a lab-grade 350 ml vacuum flask containing 150 g of water at room temperature. It is ensured that the cell is completely submerged in water and the flask is sealed. Temperature of water is also monitored using a thermocouple. During the process, heat transfers from the cell to water due to temperature difference until they both reach the same temperature. Neglecting any minor heat losses from the flask to the ambient, a statement of energy conservation for this process can be written as follows

$$m_c C_{p,c} \Delta T_c + m_w C_{p,w} \Delta T_w = 0 \quad (13)$$

Where m is mass, C_p is specific heat and ΔT is the total temperature change during the experiment. Subscripts c and w refer to the cell and water respectively. Since masses and temperatures are measured, therefore the specific heat of the cell can be determined from equation (13) based on the well-known specific heat of water.

4. Results and discussion

4.1. Numerical validation

The analytical model presented in section 2 is first validated against numerical simulations. Fig. 2 shows a comparison between the core temperature rise as a function of time predicted by the analytical model and a finite-element numerical simulation carried out in ANSYS-CFX. The boundary temperature used in this comparison is obtained from one of the experimental data on a thermal test cell illustrated in section 3. The values for Q_0 and E_a in the heat generation expression for this comparison are 5×10^{22} Wm^{-3} and 1.3×10^5 $Jmol^{-1}$ respectively. Fig. 2 shows that the analytical model and finite-element simulations are in very good agreement throughout the entire time duration, with a worst-case deviation of only 3.1% between the two. This provides a validation of the accuracy of the analytical model presented in section 2.

4.2. Experimental validation

Further validation is carried out by comparison with experimental data on a thermal test cell with known heat generation rate $Q(T)$. Two sets of experiments are carried out. In the first set, the pre-exponential factor, Q_0 is kept constant at 10^{44} Wm^{-3} while varying the activation energy E_a for heat generation in the thermal test cell through temperature-dependent heating current implemented by the LabVIEW controller. Fig. 3(a) compares the core temperature rise as a function of time measured through

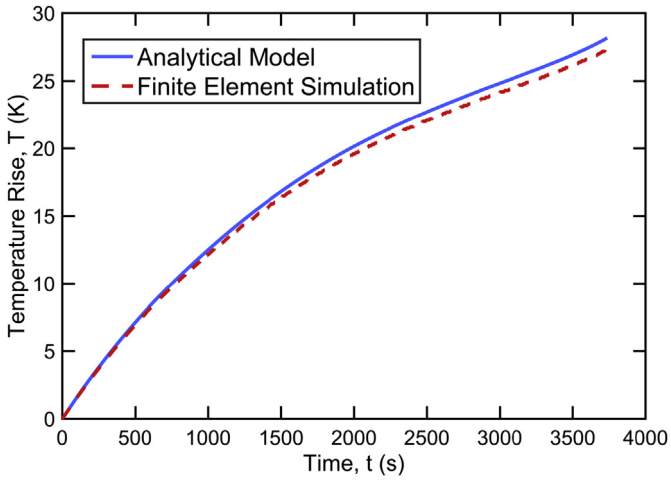

Fig. 2. Core temperature rise of the thermal test cell as a function of time predicted by the analytical model (blue curve) and a finite-element numerical simulation carried out in ANSYS-CFX (red curve). Values for Q_0 and E_a for this comparison are 5×10^{22} Wm^{-3} and 1.3×10^5 $Jmol^{-1}$ respectively. (For interpretation of the references to colour in this figure legend, the reader is referred to the web version of this article.)

experiments with the one predicted by the analytical model for different values of activation energy. Experimental data and analytical model are in very good agreement. It is seen that as the activation energy increases while keeping Q_0 constant, there is reduction in temperature rise, and thermal runaway occurs much later in time. In each case, the experimental data are found to agree well with predictions from the analytical model. The worst-case deviation between the two is found to be less than 1%. In addition to validating the analytical model, these data also show that increase in the value of activation energy results in a decrease in the slope of temperature rise as a function of time, implying that as the activation energy increases, the temperature curve will eventually begin to reach a steady state and therefore not go in thermal runaway. Both experimental data and the analytical model from section 2 follow this trend.

In the second set of experiments, Q_0 is varied while holding E_a constant at 246.9 $kJmol^{-1}$. Similar to the first set of experiments, there is very good agreement between experimental data and analytical model, as shown in Fig. 3(b), with a worst-case deviation of 1.2%. These experiments demonstrate the accuracy of the theoretical model in section 2 for computing the core temperature of the cell undergoing temperature-dependent heat generation over a wide parameter space.

4.3. Components of the core temperature

As outlined in section 2, the core temperature of the cell is computed as the sum of two different contributions, $T_{1,core}$ and $T_{2,core}$ that account for the effect of internal heat generation and outside surface temperature respectively. Under different experimental conditions, either of these two may dominate the overall core temperature. To illustrate this, Fig. 4(a) and (b) plot the core temperature rise as a function of time, along with its two components $T_{1,core}$ and $T_{2,core}$ for two different scenarios.

In the first case, the value of the activation energy is relatively small. In this case, as shown in Fig. 4(a), the core temperature is dominated by contributions from the surface temperature component $T_{2,core}$ for the first 1500 s or so. Subsequently, however, as the temperature rises, internal heat generation becomes more and more important, and as shown in Fig. 4(a), the contribution from $T_{1,core}$ begins to increase, and eventually dominate the core temperature computation, beyond 3500 s or so.

In a different scenario, however, the core temperature could be dominated throughout by only one of the two components. This is illustrated in Fig. 4(b), where the internal heat generation rate is so small that the surface temperature component $T_{2,core}$ dominates the overall core temperature throughout the duration.

These insights into the dominance of one or the other component, or the switch from one to the other as time passes are critical in designing computational approaches for determining the core temperature. For example, knowing that one of the two components is not significant under certain conditions can be used to speed up core temperature computation by not computing that component at all.

4.4. Prediction of the core temperature for past measurements of surface temperature

Several past papers have reported measurement of surface temperature of Li-ion cells during thermal runaway events caused

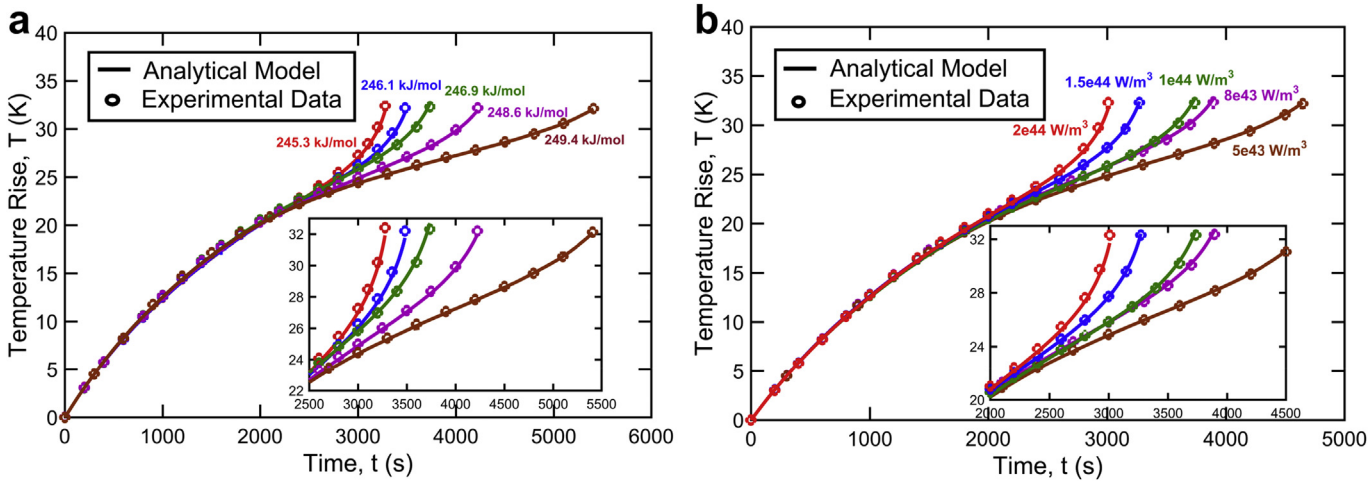

Fig. 3. Experimental validation of the analytical model. Core temperature rise as a function of time (a) for different values of activation energy E_a, while the pre exponential factor Q_0 is kept constant at 10^{44} Wm^{-3}; (b) for different values of pre-exponential constant Q_0 while activation energy E_a is kept constant at 246.9 $kJmol^{-1}$. Both experimental measurements and analytical model are presented. Subplots show zoom-ins at the later stages of each experiment when the cell begins to enter thermal runaway.

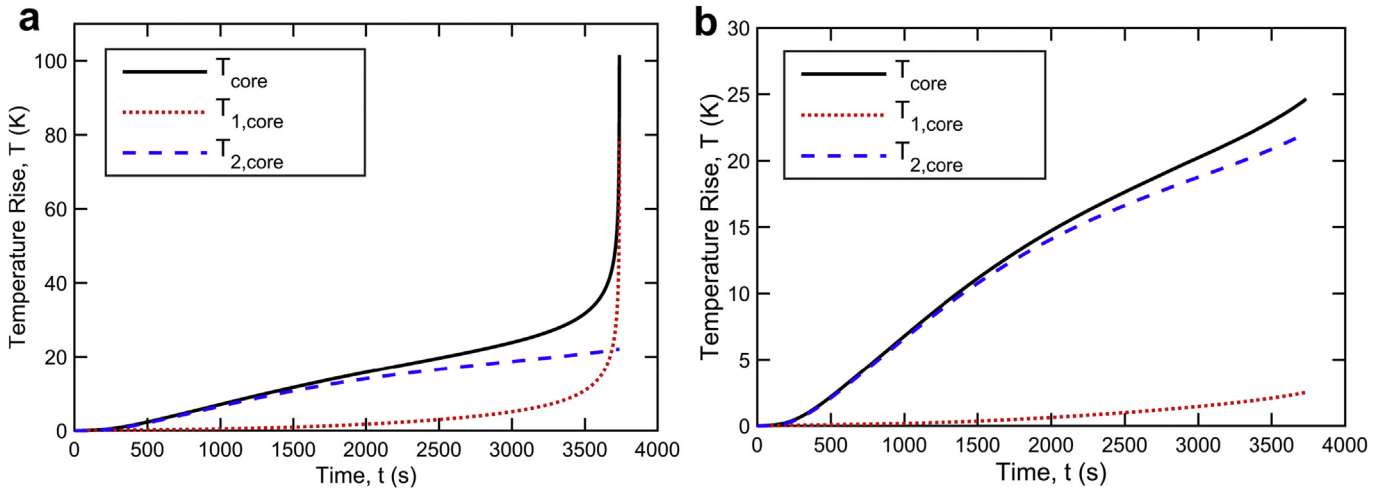

Fig. 4. Plots of the core temperature rise as a function of time, along with its two components $T_{1,core}$ and $T_{2,core}$ for (a) $Q_0 = 5 \times 10^{22}$ Wm^{-3} and $E_a = 1.1 \times 10^5$ Jmol^{-1}; (b) $Q_0 = 5 \times 10^{22}$ Wm^{-3} and $E_a = 1.1 \times 10^6$ Jmol^{-1}.

by a variety of factors such as high ambient temperature during an oven test [10,12,13]. A key drawback of these papers is the lack of information on the true temperature at the core of the cell, which may be significantly different from the reported surface temperature data.

The analytical model presented in section 2, and validated through comparison with experimental data in section 4.2 is used to determine the core temperature as a function of time and compare against surface temperature measurements reported by these papers. The primary interest here is to determine how much hotter the core is compared to the surface temperature during a thermal runaway event.

In order to do so, it is first important to define the total heat generation during thermal runaway based on chemical reaction kinetics.

Heat generation during thermal runaway has been well characterized in several past papers [7–10]. The total heat generation is the sum of heat generated due to multiple processes, including solid electrolyte interface (SEI) decomposition, negative-solvent reaction, positive-solvent reaction and electrolyte decomposition. Each of these reactions is triggered at a specific temperature. Table 1 summarizes the governing equations for heat generation for each of these processes, as well as the respective starting temperature [9]. In these equations, H, W and R refer to reaction specific heat release, material content and reaction rate, respectively. Further, m, E_a, A, c and α refer to order, activation energy, frequency factor and initial dimensionless content, respectively. Also, t_{SEI} is the initial SEI thickness. Values for various kinetic and physical parameters in the equations in Table 1 are taken from past work [9].

Total heat generation within the cell during thermal runaway is the sum of all the heat generations due to the specified reactions and is given by

$$Q_{gen} = Q_{sei} + Q_{ne} + Q_{pe} + Q_e \tag{14}$$

Core temperature of an 18650 cell undergoing thermal runaway as reported by Lopez et al. [10] is computed and compared against the reported surface temperature data. In this work, a Lithium-cobalt-oxide 18650 cell was subjected to a conventional oven test at 170 °C and surface temperature measurement using a thermocouple was reported. In order to determine the core temperature under these conditions, the reported surface temperature measurement is extracted, and used as the boundary condition for the mathematical model in section 2.

Fig. 5 plots the computed core temperature, as well as the reported surface temperature from this study. It is seen that for the first 600 s or so, the surface temperature of the cell is higher than the core temperature. This happens because the cell is initially much colder than the oven temperature, and because heat generation due to chemical reactions is not significant in the initial period. During this period, the core temperature rise is primarily due to diffusion of heat from the cell surface to the core, which is accounted for by the $T_{2,core}$ component in the analytical model. Once the cell temperature has risen significantly, chemical reactions begin to generate significant heat, resulting in sharp temperature rise. Computation of the core temperature shows that the increase in core temperature is even sharper than the measured surface temperature during the thermal runaway. The peak core temperature is found to be several hundreds of degrees Celsius higher than the surface temperature. After the thermal runaway event ends, heat diffuses from the core to the surface. The core

Table 1
Governing equations and parameters for heat generation rates of various processes responsible for thermal runaway.

Reaction	Heat Generation	Rate of Reaction	Starting Temperature
SEI Decomposition	$Q_{sei} = H_{sei} W_c R_{sei}$	$R_{sei} = A_{sei} \exp\left(-\frac{E_{a,sei}}{R_u T}\right) c_{sei}^{m,sei}$; $\frac{dc_{sei}}{dt} = -R_{sei}$	90-120 °C
Negative-Solvent Reaction	$Q_{ne} = H_{ne} W_c R_{ne}$	$R_{ne} = A_{ne}\left(-\frac{t_{sei}}{t_{sei,ref}}\right) \exp\left(-\frac{E_{a,ne}}{R_u T}\right) c_{ne}^{m,ne}$; $\frac{dc_{ne}}{dt} = -R_{ne}$	120 °C
Positive-Solvent Reaction	$Q_{pe} = H_{pe} W_p R_{pe}$	$R_{pe} = A_{pe} \alpha^{m,pe} (1-\alpha)^{m,pe} \exp\left(-\frac{E_{a,pe}}{R_u T}\right)$; $\frac{d\alpha}{dt} = R_{pe}$	170 °C
Electrolyte Decomposition	$Q_e = H_e W_e R_e$	$R_e = A_e \exp\left(-\frac{E_{a,e}}{R_u T}\right) c_e^{m,e}$; $\frac{dc_e}{dt} = -R_e$	200 °C

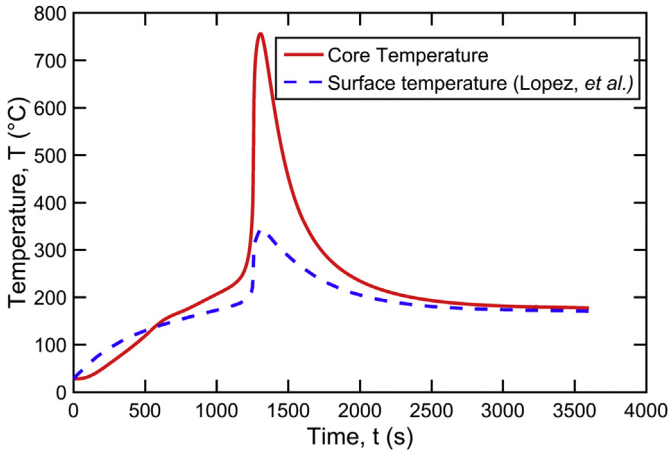

Fig. 5. Plot of the computed core temperature compared to reported surface temperature measurement [10] for a Lithium-cobalt-oxide 18650 cell undergoing an oven test.

temperature continues to be greater than the surface temperature, until at large time, the two equilibrate at the oven temperature. The significantly larger core temperature compared to the surface temperature is a critical insight into the thermal state of the cell during thermal runaway. While the surface temperature is much easier to measure, it is shown to heavily under-predict the actual temperature of the cell, which at its core may be hundreds of degrees Celsius larger than the temperature reported by a thermocouple on the outside surface.

Fig. 6 shows a similar plot of the computed core temperature for another study by Golubkov et al. [13]. In this work, an 18650 NMC ($Li\ (Ni_{0.45}\ Mn_{0.45}\ Co_{0.10})O_2$ layered oxide cathode) Li-ion cell fixed inside a heater sleeve was placed inside a heatable reactor. The cell was initially at 25 °C and heated through constant power Joule heating. Surface temperature of the cell, measured using thermocouples, is used to determine the core temperature using the analytical model in section 2. Compared to Fig. 5, the rate of temperature rise in the initial period is lower, due to slow heat diffusion into the cell. In the absence of significant internal heat generation for the first 4000 s, the core and surface temperatures remain very close to each other. In the study conducted by Lopez et al. [10] the oven was preheated to 170 °C and then the cell was inserted, whereas in this study, the temperature of the heater increases slowly, which results in only a minor difference between the core and the surface temperature during the initial period. When the cell temperature becomes large enough, significant heat begins to be generated due to exothermic reactions, which results in sharp increase in the core temperature. Similar to the previous case, the peak core temperature during thermal runaway is several hundred of degrees Celsius higher than the measured surface temperature. Once the external heating is stopped, both core and surface temperature begin to drop off, similar to the previous case.

Finally, the core temperature is also computed for thermal runaway of a $LiMn_2O_4$ Li-ion cell in an oven test [12]. In this case, the oven temperature is set to 240 °C throughout the experiment. The core temperature for this case, computed using the analytical model in section 2, as well as the reported surface temperature measurement [12] are plotted in Fig. 7. Similar to the previous two cases, this plot shows a significant difference in the computed core temperature and measured surface temperature. This shows the importance of determining the core temperature during thermal runaway events instead of relying only on surface temperature measurements, which may significantly under-predict the thermal state of the cell. During thermal runaway, the cell may be much hotter than reported by an external thermocouple, and this must be accounted for in design and run-time management of a thermal runaway situation.

As pointed out in section 2, the determination of the core temperature of the cell during thermal runaway requires information about heat generation parameters as well as thermal properties of the cell. Both of these data are available in past papers, where values of Arrhenius parameters of various processes during thermal runaway [7,8,10] as well as thermal properties of Li-ion cells [18,19] have been presented.

4.5. Effect of thermal properties on predicted temperature

Since different values for Li-ion cells thermal conductivity and specific heat have been reported in literature, a sensitivity study is conducted to understand the impact of these properties on the thermal behavior of the cell during thermal runaway.

Fig. 8(a) shows the core temperature rise as a function of time based on previously reported surface temperature [10] for different values of thermal conductivity k_r. In this case, the specific heat C_p is held constant at 715 $Jkg^{-1}K^{-1}$. Fig. 8(a) shows the effect of ±10% and ±20% variation in thermal conductivity from the baseline value of 0.2 $Wm^{-1}K^{-1}$. The temperature curves are found to be largely

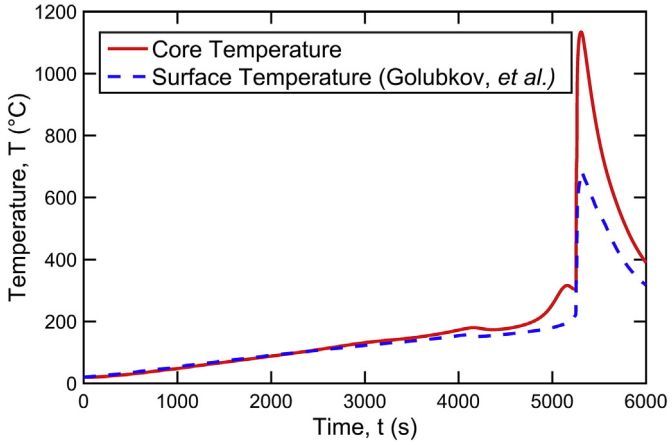

Fig. 6. Plot of the computed core temperature compared to reported surface temperature [13] for a NMC 18650 cell undergoing an oven test.

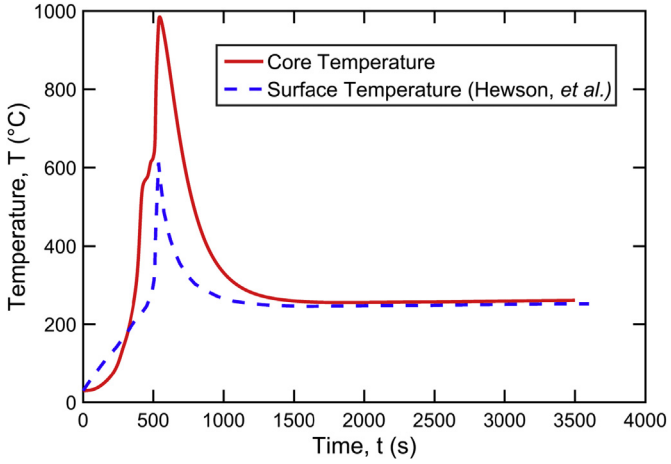

Fig. 7. Plot of the computed core temperature compared to reported surface temperature measurement for an 18650 $LiMn_2O_4$ Li-ion cell undergoing an oven test [12].

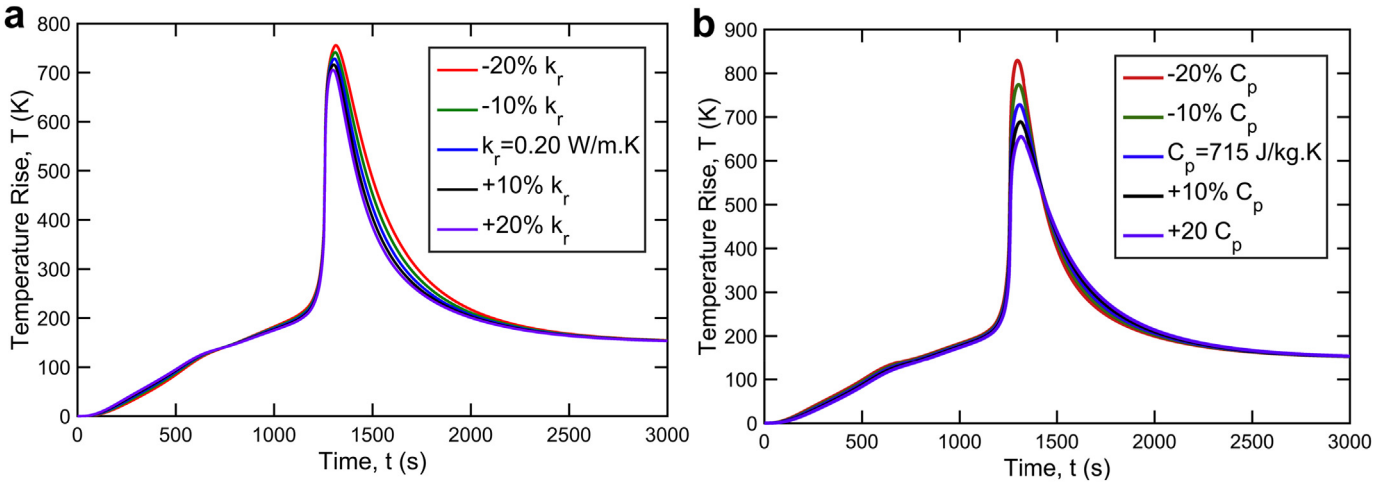

Fig. 8. (a) Core temperature rise as a function of time for different values of thermal conductivity k_r with ±10% and ±20% change from baseline, while heat capacity is held constant at 715 $Jkg^{-1}K^{-1}$; (b) core temperature as a function of time for different values of heat capacity C_p with ±10% and ±20% change from baseline, while thermal conductivity is held constant at 0.2 $Wm^{-1}K^{-1}$.

insensitive to changes in thermal conductivity. The predicted peak temperature changes by only about 2% when the thermal conductivity changes by 10%. This shows that behavior of the core temperature is not a strong function of the thermal conductivity of the cell, and uncertainties in the value of the thermal conductivity do not significantly affect the predicted temperature.

On the other hand, Fig. 8(b) compares the core temperature as a function of time for different values of specific heat C_p. In this case, the thermal conductivity is held constant at 0.2 $Wm^{-1}K^{-1}$. Similar to the previous case, ±10% and ±20% changes in C_p from the baseline value of 715 $Jkg^{-1}K^{-1}$ are considered. Unlike thermal conductivity, Fig. 8(b) shows that changes in specific heat have a relatively more significant effect on the peak temperature. While the change in temperature is not significant both before and after thermal runaway, the peak temperature rise around thermal runaway changes by 7% with a 10% change in specific heat. In general, the predicted peak temperature rise increases with reduction in heat capacity, which is along expected lines. This shows that accurate information about C_p is much more critical than k_r.

Due to the critical importance of C_p on thermal behavior of the cell during thermal runaway, experiments are carried out to measure the specific heat of an 18650 Li-ion cell, as described in section 3. Supplementary Fig. 1 plots temperature as a function of time for both the Li-ion cell and water during these experiments. It is found that once the cell is submerged in water, the cell temperature reduces while the water temperature rises. After a short time, both reach a thermal equilibrium. Based on measurements of change in temperature for cell and water, their thermal masses and the specific heat of water, specific heat of the cell is determined from equation (13). The specific heat of the 18650 Li-ion cell is found to be 715 $J\ kg^{-1}K^{-}$.[1]

5. Conclusions

This work develops an analytical heat transfer model to determine the core temperature of a Li-ion cell undergoing thermal runaway based on surface temperature measurement. The technique is suitable for determining the core temperature as a function of time for a variety of experimental conditions where the surface temperature has been measured. Results show that the maximum core temperature during thermal runaway is several hundreds of degrees Celsius higher than the surface temperature. This demonstrates the critical importance of the core temperature of the cell during thermal runaway. The accuracy of the technique depends on chemical kinetics data during thermal runaway, as well as on thermophysical properties of the cell, particularly its specific heat. This work provides a new fundamental insight into the thermal behavior of Li-ion cells during thermal runaway, which is not possible through surface temperature measurement alone. It is expected that information about the core temperature of the cell during thermal runaway, determined by the technique described here may help improve the fundamental understanding of thermal runaway, as well as help design practical tools to predict the thermal state of the cell so that thermal runaway could be mitigated.

Acknowledgments

This material is based upon work supported by CAREER Award No. CBET-1554183 from the National Science Foundation.

Appendix A. Supplementary data

Supplementary data related to this article can be found at https://doi.org/10.1016/j.jpowsour.2017.09.086.

References

[1] V. Etacheri, R. Marom, R. Elazari, G. Salitra, D. Aurbach, Energy Environ. Sci. 4 (2011) 3243, https://doi.org/10.1039/c1ee01598b.
[2] J.B. Goodenough, K.-S. Park, J. Am. Chem. Soc. 135 (2013) 1167, https://doi.org/10.1021/ja3091438.
[3] B. Scrosati, J. Garche, J. Power Sources 195 (2010) 2419–2430, https://doi.org/10.1016/j.jpowsour.2009.11.048.
[4] K. Shah, N. Balsara, S. Banerjee, M. Chintapalli, A.P. Cocco, W.K.S. Chiu, et al., J. Electrochem. Energy Conv. Storage 14 (2017) 020801, https://doi.org/10.1115/1.4036456.
[5] K. Shah, V. Vishwakarma, A. Jain, J. Electrochem. Energy Conv. Storage 13 (2016) 030801, https://doi.org/10.1115/1.4034413.
[6] T.M. Bandhauer, S. Garimella, T.F. Fuller, J. Electrochem. Soc. 158 (2011) R1, https://doi.org/10.1149/1.3515880.
[7] A. Melcher, C. Ziebert, M. Rohde, H. Seifert, Energies 9 (2016) 292, https://doi.org/10.3390/en9040292.
[8] R. Spotnitz, J. Franklin, J. Power Sources 113 (2003) 81–100, https://doi.org/10.1016/s0378-7753(02)00488-3.
[9] G.-H. Kim, A. Pesaran, R. Spotnitz, J. Power Sources 170 (2007) 476–489, https://doi.org/10.1016/j.jpowsour.2007.04.018.
[10] C.F. Lopez, J.A. Jeevarajan, P.P. Mukherjee, J. Electrochem. Soc. 162 (2015) A2163, https://doi.org/10.1149/2.0751510jes.
[11] K. Shah, D. Chalise, A. Jain, J. Power Sources 330 (2016) 167–174, https://doi.org/10.1016/j.jpowsour.2016.08.133.

[12] J. Hewson, R. Shurtz, Energy Storage Systems Safety & Reliability Workshop, Sante Fe, NM, 2017.
[13] A.W. Golubkov, D. Fuchs, J. Wagner, H. Wiltsche, C. Stangl, G. Fauler, et al., RSC Adv. 4 (2014) 3633–3642, https://doi.org/10.1039/c3ra45748f.
[14] H. Maleki, J. Electrochem. Soc. 146 (1999) 3224, https://doi.org/10.1149/1.1392458.
[15] E. Roth, D. Doughty, J. Power Sources 128 (2004) 308–318, https://doi.org/10.1016/j.jpowsour.2003.09.068.
[16] J. Dahn, E. Fuller, M. Obrovac, U. Vonsacken, Solid State Ionics 69 (1994) 265–270, https://doi.org/10.1016/0167-2738(94)90415-4.
[17] D. Macneil, Z. Lu, Z. Chen, J. Dahn, J. Power Sources 108 (2002) 8–14, https://doi.org/10.1016/s0378-7753(01)01013-8.
[18] S. Drake, M. Martin, D. Wetz, J. Ostanek, S. Miller, J. Heinzel, et al., J. Power Sources 285 (2015) 266–273, https://doi.org/10.1016/j.jpowsour.2015.03.008.
[19] Y. Ye, L.H. Saw, Y. Shi, K. Somasundaram, A.A. Tay, Electrochim. Acta 134 (2014) 327–337, https://doi.org/10.1016/j.electacta.2014.04.134.
[20] J. Jeevarajan, Safety of commercial Lithium-ion cells and batteries, in: G. Pistoia (Ed.), Lithium-ion Batteries, 2014, pp. 387–407, https://doi.org/10.1016/b978-0-444-59513-3.00017-0.
[21] D. Anthony, D. Sarkar, A. Jain, Sci. Rep. 6 (2016), https://doi.org/10.1038/srep35886, 35886:1.
[22] D. Anthony, D. Wong, D. Wetz, A. Jain, Int. J. Heat. Mass Transf. 111 (2017) 223–231, https://doi.org/10.1016/j.ijheatmasstransfer.2017.03.095.
[23] D.V. Forgez, G. Do, M. Friedrich, C. Morcrette, J. Delacourt, Power Sources 195 (2010) 2961–2968, https://doi.org/10.1016/j.jpowsour.2009.10.105.
[24] J.B. Robinson, J.A. Darr, D.S. Eastwood, G. Hinds, P.D. Lee, P.R. Shearing, et al., J. Power Sources 252 (2014) 51–57, https://doi.org/10.1016/j.jpowsour.2013.11.059.
[25] S. Drake, D. Wetz, J. Ostanek, S. Miller, J. Heinzel, A. Jain, J. Power Sources 252 (2014) 298–304, https://doi.org/10.1016/j.jpowsour.2013.11.107.
[26] S. Novais, M. Nascimento, L. Grande, M. Domingues, P. Antunes, N. Alberto, et al., Sensors 16 (2016) 1394, https://doi.org/10.3390/s16091394.
[27] R. Srinivasan, B.G. Carkhuff, M.H. Butler, A.C. Baisden, Electrochim. Acta 56 (2011) 6198–6204, https://doi.org/10.1016/j.electacta.2011.03.136.
[28] G. Zhang, L. Cao, S. Ge, C.-Y. Wang, C.E. Shaffer, C.D. Rahn, J. Electrochem. Soc. 161 (2014), https://doi.org/10.1149/2.0051410jes.
[29] R.A. Leising, M.J. Palazzo, E.S. Takeuchi, K.J. Takeuchi, J. Electrochem. Soc. 148 (2001) A838–A844.
[30] D.W. Hahn, M.N. Özişik, Heat Conduction, third ed., John Wiley & Sons, Hoboken, New Jersey, 2012.
[31] F.P. Incropera, D.P. DeWitt, T.L. Bergman, A.S. Levine, Introduction to Heat Transfer, fifth ed., John Wiley & Sons, 2006.